Research Square

Preprints are preliminary reports that have not undergone peer review.
They should not be considered conclusive, used to inform clinical practice,
or referenced by the media as validated information.

Protocatechuic aldehyde modulates hepatic cholesterol homeostasis by regulating LDL uptake and bile acid synthesis

Yunying Li

2594903717@qq.com

Yunnan University of Traditional Chinese Medicine

Mingli Yan

Yunnan University of Traditional Chinese Medicine

Ziqi Liu

Yunnan University of Traditional Chinese Medicine

Xiaomeng Zhang

Yunnan University of Traditional Chinese Medicine

Xiaoyu Tan

Yunnan University of Traditional Chinese Medicine

Shiyao Xu

Yunnan University of Traditional Chinese Medicine

Yuanhan Li

Yunnan University of Traditional Chinese Medicine

Qing Lin

Yunnan University of Traditional Chinese Medicine

Yujing Li

Kunming Health Vocational College

Fangyan He

Yunnan University of Traditional Chinese Medicine

Research Article

Keywords: Protocatechuic aldehyde, Cholesterol metabolism, Molecular docking, Molecular dynamics simulation, Atherosclerosis

Posted Date: July 7th, 2026

DOI: https://doi.org/10.21203/rs.3.rs-10185784/v1

License: This work is licensed under a Creative Commons Attribution 4.0 International License.
Read Full License

Additional Declarations: No competing interests reported.

Abstract

Dysregulated cholesterol metabolism is a key determinant of atherosclerotic initiation and progression. Protocatechuic aldehyde (PAL), a phenolic aldehyde with diverse pharmacological properties, shows pronounced anti-atherosclerotic effects, yet its influence on hepatic cholesterol homeostasis remains insufficiently defined. Purpose : this study investigated the regulatory role of PAL in hepatic cholesterol metabolism in Sprague Dawley rats fed a high-fat diet (HFD) to induce hepatic cholesterol imbalance. Methods : following 2 weeks of HFD feeding, PAL (20 mg/kg/d) was administered via gavage for 6 weeks, after which hepatic cholesterol metabolism was assessed through biochemical profiling, histopathology, lipid deposition analysis, molecular docking, and molecular dynamics simulations. Results : PAL administration markedly attenuated hepatic lipid accumulation and mitigated HFD-induced structural injury. Serum and hepatic concentrations of total cholesterol, triglycerides, and low-density lipoprotein cholesterol declined substantially, accompanied by an elevation in high-density lipoprotein cholesterol. Serum total bile acid levels also declined, indicating broad lipid-modulating activity. Molecular docking and dynamics simulations indicated stable binding of PAL to cholesterol-regulatory targets. These *in silico* predictions were corroborated by elevated expression of LDLR, LXRα, and CYP7A1, and reduced expression of PCSK9, as confirmed by real-time quantitative polymerase chain reaction and immunohistochemical analysis. Conclusion : PAL ameliorates hepatic cholesterol dysregulation through coordinated modulation of uptake, conversion, and excretory pathways, underscoring its therapeutic potential for atherosclerosis.

Highlights

• PAL effectively alleviates liver lipid deposition and tissue structure damage induced by a high-fat diet.

• PAL significantly reduces the levels of total cholesterol, triglycerides and low-density lipoprotein in serum and liver.

• Molecular docking and kinetic simulations indicate that PAL can stably bind to cholesterol regulatory targets.

• PAL improves cholesterol homeostasis by up-regulating the expression of key genes such as LXRα and CYP7A1.

• PAL has demonstrated potential in treating atherosclerosis through multi-pathway synergistic regulation.

1. Introduction

Atherosclerosis (AS) is a progressive inflammatory disease of the arterial wall, primarily driven by cholesterol deposition within the intimal layer and recognized as a major cause of cardiovascular mortality and disability worldwide(Soehnlein and Libby 2021; Ajoolabady et al. 2024). Accumulation of

cholesterol in the vascular intima initiates a cascade of chronic inflammatory responses, including endothelial activation and the upregulation of adhesion molecules that recruit circulating monocytes. These monocytes infiltrate the endothelium, differentiate into macrophages, and internalize lipids to transform into foam cells. Apoptosis of foam cells contributes to necrotic core formation, thereby accelerating lesion development and plaque destabilization(Lightbody et al. 2020; Xu et al. 2022; Wang et al. 2022; Pickett et al. 2023). With disease progression, ongoing lipid accumulation and inflammatory activity lead to intraplaque calcification, increasing the risk of rupture and acute cardiovascular events(Shi et al. 2020; Cai et al. 2023). Aberrant cholesterol metabolism is thus central to AS through the promotion of macrophage and foam cell accumulation in the arterial wall(Lightbody et al. 2020; Guo et al. 2023), highlighting cholesterol homeostasis as a critical therapeutic target.

Protocatechuic aldehyde (PAL), a natural polyphenol abundant in medicinal plants such as *Salvia miltiorrhiza* and *Gastrodia elata*, exhibits diverse pharmacological effects, including antioxidant, anti-inflammatory, and anti-aging activities(Guo et al. 2022). Recent studies have shown that PAL enhances the atherosclerotic plaque stability by preserving pericyte integrity and reducing pericyte loss(Dave et al. 2013; Zhang et al. 2023). However, the potential of PAL to modulate hepatic cholesterol metabolism as a mechanism for attenuating AS has not been established. This study examined the regulatory effects of PAL on hepatic cholesterol homeostasis in a high-fat diet (HFD)-induced rat model, providing initial evidence of its therapeutic potential in AS and establishing a basis for further investigation. Findings showed that PAL modulated liver cholesterol metabolism by altering both uptake and efflux pathways, supporting its relevance as a candidate for AS intervention.

2. Materials and Methods

2.1. Materials

PAL (purity ≥ 98%) was purchased from J&K Scientific (Beijing, China). Simvastatin was obtained from Lukang Pharmaceutical Group Saite Co., Ltd. (Shandong, China). High-fat diet (HFD) feed was purchased from Keao Xieli Feed Co., Ltd. (Beijing, China). Commercial assay kits for total bile acid (TBA), total cholesterol (TC), triglycerides (TG), high-density lipoprotein cholesterol (HDL-C), and low-density lipoprotein cholesterol (LDL-C) were purchased from Jiancheng Bioengineering Institute (Nanjing, China).

2.2. Animals

Specific pathogen-free (SPF) male Sprague Dawley (SD) rats (6 weeks old, 200–220 g; Certificate No.: 110324220106101646) were supplied by Sibeifu (Beijing) Biotechnology Co., Ltd. (China) (License No.: SCXK (Jing) 2019-0010). The rats were housed under standard conditions (23.5 ± 2.0°C, relative humidity 55% ± 5%, 12-h light/dark cycle) with *ad libitum* access to food and water. After a 7-day acclimatization period, rats were randomly allocated into a control group (n = 6; normal diet) and an HFD group (n = 18, high-fat diet). After 2 weeks, blood was collected from all animals without prior fasting to measure serum TC levels. Based on these measurements, the HFD-fed rats were subdivided into three groups:

HFD model, simvastatin (7.2 mg/kg), and PAL (20 mg/kg) groups. Each treatment group was administered the corresponding drugs via oral gavage at a volume of 10 mL/kg, while the control and model groups were administered an equal volume of double-distilled water. Treatments were continued for 6 weeks. Body weight was recorded weekly. At the end of the treatment period, animals were fasted for 12 h, anesthetized, and sacrificed. Blood and liver samples were collected from the abdominal aorta for further analysis. All procedures and experiments were approved by the Experimental Animal Ethics Committee of Yunnan University of Traditional Chinese Medicine (Approval No.: R-062022137).

2.3. Serum biochemical analysis

Blood was collected from the orbital sinus of mice and serum was subsequently isolated. Serum TBA, TC, TG, LDL-C, and HDL-C levels were quantified using commercial assay kits from Nanjing Jiancheng Bioengineering Institute (China) in accordance with the manufacturer's protocols. Absorbance was measured with a SpectraMax I3X microplate reader.

2.4. Hepatic biochemical analysis

Excised liver tissue was washed with ice-cold saline and blotted dry. The right lobe was sectioned, and approximately 50 mg of tissue was weighed and homogenized in 0.9% sodium chloride solution (1:9 ratio) using a SCIENTZ-48 high-throughput tissue grinder. Homogenates were centrifuged at 3 500 rpm for 10 min in a low-temperature high-speed centrifuge, and the resulting supernatant was collected. TC, TG, LDL-C, and HDL-C concentrations were determined in the 10% liver homogenate according to the corresponding assay kit instructions.

2.5. Histopathological analysis

Liver tissue reserved from biochemical analysis was fixed in 4% paraformaldehyde (v/v) solution. Samples were dehydrated for 12 h in a fully automatic vacuum dehydrator and embedded in paraffin using a tissue embedding system. Sections (4 μm) were prepared using a microtome, dewaxed, stained with hematoxylin and eosin (H&E), mounted, and imaged using a digital slide-scanning system. For lipid deposition analysis, additional liver tissue was processed similarly, followed by Oil Red O staining. Sections were differentiated, counterstained with hematoxylin, rinsed, blued, mounted, and scanned to assess hepatic lipid accumulation.

2.6. Molecular docking

Three-dimensional structures of the target proteins LDLR, PCSK9, LXRα, and CYP7A1 were downloaded in "pdb" format from the Protein Data Bank (PDB) database. The structure of PAL was obtained in "sdf" format from the PubChem database. Prior to docking, all receptor proteins were preprocessed using PyMOL v2.5 by removing water molecules, salt ions, and bound ligands. Processed structures were converted to PDBQT format using AutoDockTools to meet the input requirements of AutoDock Vina v1.1.2. Molecular docking was conducted using default parameters, and the highest-affinity binding pose was selected for each target. Docked complexes were visualized using PyMOL v2.5.

2.7. Molecular dynamics simulation

Molecular dynamics simulations were performed using GROMACS 2022 for 100 ns. The CHARMM36 force field was applied to the proteins, and ligand topology was generated using the AFF2 force field. Each protein-ligand complex was placed in a cubic box filled with TIP3P water molecules, with a minimum distance of 1.2 nm from the complex to the box edge. Periodic boundary conditions were applied in all directions. Electrostatic interactions were calculated using the Particle Mesh Ewald (PME) algorithm. Energy minimization and system equilibration were performed using the isothermal-isochoric and isothermal-isobaric ensembles (100 000 steps each), with a coupling constant of 0.1 ps. The system was equilibrated for 100 ps before production runs. Both van der Waals and Coulomb interactions were calculated with a cutoff of 1.0 nm. Simulations were conducted at a constant temperature (310 K) and pressure (1 bar).

2.8. Quantitative real-time polymerase chain reaction (qPCR)

Approximately 45–55 mg of liver tissue was used for total RNA extraction according to the instructions of the RNA extraction kit. RNA concentration was measured, and equal quantities of RNA were subjected to reverse transcription and PCR amplification. Raw data were collected and analyzed using the QuantStudio™ Design & Analysis Software v1.5.2. Relative mRNA expression was calculated using the $2^{-\triangle\triangle CT}$ method. Briefly, $\triangle$CT was first obtained (CT target gene − CT reference gene), followed by $\triangle\triangle$CT ($\triangle$CT experimental group − $\triangle$CT normal group), with the fold change in mRNA expression in the experimental group relative to the normal group calculated using $F = 2^{-\triangle\triangle CT}$(Galeotti et al. 2023; Jeong et al. 2025). Primer sequences for each target gene are shown in Table 1.

Table 1
Primer sequences of target genes

Oligo	Sequence (5’-3’)
LDLR	F: GGACAAGTCGGACGAGGAGAAC
	R: CGGTCACACTGGCGGCTAC
PCSK9	F: TGGAGCAACGGCGGAAGG
	R: CGAGGACGGAGACTACGAAGAG
LXRα	F: GGAGACCAGGGAGGCAACAC
	R: GGCTGTAGGCTCGGATGACTC
CYP7A1	F: AGGTCTCTGAACTGATCCGTCTAC
	R: GAATAGCGAGGTGCGTCTTGG

2.9. Immunohistochemical analysis

Paraffin-embedded liver tissues were sectioned, subjected to antigen retrieval, endogenous peroxidase quenching, and blocking. Sections were incubated with primary antibodies against LDLR (1:1 000), LXRα

(1:1 000), CYP7A1 (1:1 000), and PCSK9 (1:400), followed by incubation with appropriate secondary antibodies. Detection was performed using DAB chromogenic substrate, and nuclei were counterstained. After dehydration and mounting, slides were scanned to assess the relative expression levels of the target proteins.

2.10. Statistical analysis

All data obtained in this experiment were analyzed using IBM SPSS Statistics 27, with results expressed as mean ± standard deviation (SD). Normality of distribution was assessed prior to further analysis. For non-normally distributed data, non-parametric tests were applied. For normally distributed data, homogeneity of variance was evaluated. If variance was homogeneous, one-way analysis of variance (ANOVA) followed by Dunnett's post hoc test was performed. If variance was not homogeneous, the Kruskal-Wallis test was used. Statistical significance was defined as $P < 0.05$. All graphs were plotted using GraphPad Prism software.

3. Results

3.1. PAL attenuates hepatic steatosis in HFD-fed rats

Baseline body weights were comparable across groups, confirming successful randomization. From the second week of PAL administration through the end of the 8-week intervention, rats in the HFD group exhibited a marked increase in body weight (Fig. 2A). At the treatment endpoint, body weight in the HFD groups remained significantly elevated compared to the normal diet group ($P < 0.01$), whereas PAL-treated rats (20 mg/kg/d) showed a significant reduction in body weight relative to untreated HFD-fed rats ($P < 0.05$) (Fig. 2B). Histological assessment via Oil Red O and H&E staining revealed excessive lipid droplet accumulation, vacuolar degeneration, and inflammatory infiltration in the livers of HFD-fed rats. PAL treatment effectively reduced hepatic lipid accumulation and mitigated pathological alterations associated with steatosis (Fig. 2C–D).

3.2. PAL regulates cholesterol metabolism in HFD-fed rats

Following 6 weeks of treatment, rats fed a HFD exhibited significant elevations in serum TC, TG, LDL-C, and TBA levels ($P < 0.001$), along with a marked reduction in HDL-C levels ($P < 0.001$) compared to the control group. In liver tissue, levels of TC, TG, LDL-C, and HDL-C were also significantly elevated ($P < 0.001$, $P < 0.05$). PAL administration markedly attenuated the elevations in serum TC, LDL-C, and TG (Fig. 3A–C) and also significantly increased HDL-C levels (Fig. 3D). The observed rise in hepatic HDL-C levels in the HFD group ($P < 0.05$) may reflect an endogenous response to HFD challenge. Compared to the HFD-fed group, PAL treatment significantly lowered both serum and hepatic TC, TG, and LDL-C levels ($P < 0.05$, $P < 0.001$), while significantly enhancing HDL-C concentrations ($P < 0.05$, $P < 0.001$) (Fig. 3F–I). Serum TBA levels were also significantly reduced by PAL intervention (Fig. 3E). Collectively, these findings indicate that PAL exerts potent lipid-lowering effects under hyperlipidemic conditions and may contribute to the prevention of AS.

Figure 3. PAL modulates cholesterol metabolism in HFD-fed rats. Serum levels of TC (A), TG (B), LDL-C (C), HDL-C (D), and TBA (E). Hepatic levels of TC (F), TG (G), LDL-C (H), and HDL-C (I). Data are presented as mean ± SD (n = 6). $^{*}P < 0.05$, $^{***}P < 0.001$ vs. control group; $^{\#}P < 0.05$, $^{\#\#}P < 0.01$, $^{\#\#\#}P < 0.001$ vs. HFD group.

3.3. Molecular docking validation

Precise molecular docking was performed to evaluate the interaction between PAL and four key targets involved in cholesterol metabolism: PCSK9, LDLR, LXRα, and CYP7A1. The calculated binding energies were − 5.5 kcal/mol for PCSK9, − 6.1 kcal/mol for LDLR, − 5.6 kcal/mol for LXRα, and − 5.6 kcal/mol for CYP7A1 (Table 2), indicating favorable binding affinity. These results suggest that PAL can stably interact with all four targets (Fig. 4A–D).

Table 2
Molecular docking results of PAL with key targets in cholesterol metabolism

Target	Binding energy (kcal/mol)
PCSK9	−5.5
LDLR	−6.1
LXRα	−5.6
CYP7A1	−5.6

3.4. Molecular dynamics simulation

Molecular dynamics simulations were conducted to assess the stability of PAL binding to PCSK9, LDLR, LXRα, and CYP7A1. Root mean square deviation (RMSD) was used as a primary indicator for evaluating the structural stability of each ligand-target protein complex, with a lower average RMSD value indicating tighter ligand binding and enhanced complex stability(Shi et al. 2023; Yang et al. 2024). As shown in Fig. 5A, the PCSK9-PAL complex reached equilibrium by 10 ns and fluctuated around 2.7Å. The LDLR-PAL complex stabilized after 90 ns, with fluctuations near 2.4Å. The LXRα-PAL complex achieved equilibrium at 20 ns and fluctuated around 2Å. The CYP7A1-PAL complex reached equilibrium after 90 ns and fluctuated around 3.6Å. These results indicate that PAL can form stable interactions with all four target proteins.

Solvent accessible surface area (SASA) was calculated to evaluate changes in the protein-ligand interface microenvironment(Hosseini Faradonbeh et al. 2025). All four complexes displayed slight SASA fluctuations that gradually stabilized over the simulation period (Fig. 5B), suggesting that PAL binding can influence the surface microenvironment.

The radius of gyration (Rg) reflects the overall compactness of a molecular system, with larger variation indicating structural expansion(Jimmy et al. 2023). Analysis of the PCSK9-PAL, LDLR-PAL, LXRα-PAL,

and CYP7A1-PAL complexes showed relatively stable Rg fluctuations throughout the simulation, suggesting no significant expansion or contraction occurred during the simulation period (Fig. 5C).

Hydrogen bond formation was also evaluated as an indicator of complex stability, with a significant increase indicating a more stable system(Park and Workun; Vinolo-Gil et al.). The PCSK9-PAL, LDLR-PAL, and LXRα-PAL complexes formed an average of approximately three hydrogen bonds (ranging from 0–7, 0–5, and 0–5, respectively), while the CYP7A1-PAL complex formed around two hydrogen bonds (ranging from 0–6) (Fig. 5D), indicating favorable and sustained hydrogen bonding interactions.

Root mean square fluctuation (RMSF) analysis was performed to assess residue-level flexibility across the complexes, with smaller values suggesting a more stable complex system(Alugoju et al. 2024; Guerguer et al. 2025). Most RMSF values remained below 4 Å, indicating lower flexibility and higher stability (Fig. 5E–H).

Overall, the PCSK9-PAL, LDLR-PAL, LXRα-PAL, and CYP7A1-PAL complexes exhibited stable conformations, favorable binding energies, consistent hydrogen bonding, and low residue fluctuation throughout the 100 ns simulations, demonstrating that PAL maintained stable interactions with key regulators of cholesterol metabolism.

3.5. PAL regulates cholesterol metabolism by influencing LDLR, LXRα, CYP7A1, and PCSK9 mRNA expression in the liver

Quantitative PCR analysis revealed that hepatic mRNA expression levels of PCSK9, LDLR, LXRα, and CYP7A1 were significantly reduced in the HFD group compared with the control group ($P < 0.001$, $P < 0.05$). PAL treatment significantly downregulated PCSK9 expression ($P < 0.001$), while the mRNA expression levels of LDLR, LXRα, and CYP7A1 were significantly upregulated ($P < 0.05$, $P < 0.001$) (Fig. 6A–D).

Figure 6. PAL modulates cholesterol metabolism by influencing hepatic mRNA levels of LDLR, LXRα, CYP7A1, and PCSK9. Relative mRNA expression levels of PCSK9 (A), LDLR (B), LXRα (C), and CYP7A1 (D) in the liver. Data are presented as mean ± SD. $^{*}P < 0.05$, $^{***}P < 0.001$ vs. control group; $^{\#}P < 0.05$, $^{\#\#}P < 0.01$, $^{\#\#\#}P < 0.001$ vs. HFD group.

3.6. PAL regulates cholesterol metabolism by influencing LDLR, LXRα, CYP7A1, and PCSK9 protein levels in the liver

Hepatic expression of the PCSK9 protein was significantly increased in the HFD group compared with the control group, while the LDLR, LXRα, and CYP7A1 expression levels were markedly decreased. PAL intervention significantly reduced PCSK9 expression and restored LDLR, LXRα, and CYP7A1 protein levels (Fig. 7A–D).

4. Discussion

AS remains the principal cause of cardiovascular morbidity and mortality worldwide, with excessive cholesterol accumulation representing a major risk factor for both cardiovascular and metabolic disorders(Magnussen et al. 2023; Chen et al. 2024a; Toth and Banach 2024). Although statins are routinely prescribed, their application is limited by adverse effects such as rhabdomyolysis and hepatotoxicity(Li et al. 2025a; Bahardoust et al. 2025). Natural compounds with diverse chemical scaffolds and cardiovascular protective properties have attracted increasing attention as potential lipid-lowering agents. This study evaluated the regulatory effects of PAL on hepatic cholesterol metabolism in HFD-fed rats. PAL treatment inhibited lipid deposition in the liver, reduced systemic and hepatic lipid levels, and decreased serum TBA levels. Mechanistic investigations revealed that PAL modulated two key aspects of cholesterol regulation, notably hepatic cholesterol uptake and bile acid-mediated excretory transport. These findings support the potential of PAL as a therapeutic candidate for delaying AS progression.

As the central organ for cholesterol homeostasis, the liver primarily clears circulating LDL-C via LDL receptors (LDLRs) expressed on hepatocyte basolateral membranes(Clifford et al. 2023). However, binding of PCSK9 to LDLRs promotes receptor degradation, impeding its recycling to the cell surface and thereby reducing hepatic LDL-C clearance while elevating plasma LDL-C concentrations—a pathological feature that exacerbates AS(Kong et al. 2022; Hummelgaard et al. 2023). Consequently, inhibition of PCSK9 expression and stabilization of LDLRs are crucial strategies for restoring hepatic LDL-C uptake and lowering plasma cholesterol burden(Handelsman and Lepor 2018; Chen et al. 2024b). In this study, PAL administration effectively suppressed hepatic PCSK9 expression while enhancing LDLR protein levels, suggesting a favorable impact on LDL-C clearance. Reverse cholesterol transport (RCT) is the primary pathway for eliminating excess cholesterol from the body, mobilizing cholesterol from peripheral tissues to the liver. This process culminates in hepatic conversion of cholesterol into bile acids or other metabolic derivatives for excretion and is transcriptionally regulated by LXRα[37–39]. Upon activation, LXRα up-regulates the expression of CYP7A1, thereby promoting bile acid synthesis and facilitating cholesterol elimination, ultimately reducing hepatic TC levels [40,41]. Notably, CYP7A1 induction has also been associated with increased expression of LDLR, suggesting a potential synergistic mechanism in enhancing cholesterol clearance. The present study showed that PAL treatment significantly increased hepatic expression of both LXRα and CYP7A1[42,43]. These findings suggest that PAL may modulate hepatic cholesterol homeostasis by concurrently regulating PCSK9/LDLR-mediated LDL uptake and LXRα/CYP7A1-driven bile acid synthesis and excretion.

This study still has several limitations to mention. First, the mechanistic insights derived from this study remain associative rather than causative. Although changes in LDLR, LXRα, CYP7A1, and PCSK9 were observed following PAL treatment, it cannot be conclusively determined whether PAL exerts its cholesterol-lowering effects by directly regulating these targets. Functional validation via genetic perturbation—such as loss-of-function or gain-of-function experiments—will be necessary to establish mechanistic causality. For example, demonstrating that LXRα knockdown in hepatocytes attenuates PAL-induced CYP7A1 upregulation and cholesterol efflux would provide compelling evidence that LXRα

is a key target through which PAL exerts its functions. Second, although PAL significantly modulated cholesterol homeostasis and exhibited lipid-lowering activity in HFD-fed rats, direct anti-atherosclerotic effects were not assessed. To further substantiate the therapeutic relevance of PAL, future studies should employ classical AS models, such as ApoE$^{-/-}$ mice, and quantify various endpoints, including lesion burden, plaque area, and plaque stability. Specifically, histological analyses of the aortic arch, aortic root, and brachiocephalic trunk using Oil Red O and H&E staining could quantify lipid accumulation and structural disruption, with plaque burden expressed as a percentage of vascular or luminal area(Dou et al. 2019; Ding et al. 2019; Wei et al. 2021). Plaque stability could also be assessed by detecting macrophage markers (e.g., CD68/CD36) and matrix metalloproteinases (e.g., MMP-2, MMP-9)(Li et al. 2025b). In addition to cholesterol dysregulation, oxidative stress and inflammation contribute to AS pathophysiology(Jia et al. 2025). Therefore, future investigations should incorporate markers of oxidative and inflammatory stress, such as malondialdehyde (MDA), superoxide dismutase (SOD), tumor necrosis factor-α (TNF-α), and interleukin-1β (IL-1β) levels, in both liver and serum. Such comprehensive profiling would allow a more complete assessment of the therapeutic efficacy of PAL against AS.

5. Conclusions

This study demonstrated that PAL effectively maintains homeostasis of hepatic cholesterol metabolism by concurrently modulating cholesterol uptake and excretory transport pathways. This dual-action mechanism highlights the therapeutic potential of PAL as a candidate for AS intervention.

Abbreviations

Abbreviations	
PAL	Protocatechuic aldehyde
HFD	High-fat diet
LDLR	Low-density lipoprotein receptor
LXRα	Hepatic X receptor α
CYP7A1	Cholesterol 7α-hydroxylase
PCSK9	Proprotein convertase subtilisin/Kexin type 9
AS	Atherosclerosis
TBA	Total bile acid
TC	Total cholesterol
TG	Triglycerides
HDL-C	High-density lipoprotein cholesterol
LDL-C	Low-density lipoprotein cholesterol
RMSD	Root mean square deviation
SASA	Solvent accessible surface area
RMSF	Root mean square fluctuation
Rg	Radius of gyration
RCT	Reverse cholesterol transport

Declarations

Data availability statement

Data will be made available on request.

Funding

This study was supported by the National Natural Science Foundation of China (82360784), Key Project of Basic Research Special Program of Yunnan Provincial Science and Technology Department (202501AS070142), and Key Project of Yunnan Provincial Science and Technology Department Science and Technology Plan-Traditional Chinese Medicine Joint Special Program-Key Project (202101AZ070001-009).

Declaration of competing interests

The authors declare no known competing financial interests or personal relationships that could be perceived as influencing the work reported in this article.

CRediT authorship contribution statement

Yunying Li: Drafting, visualization, data organization. Mingli Yan: Visualization, research, data organization. Ziqi Liu: Visualization, research, data organization. Xiaomeng Zhang: Visualization, research, data organization. Xiaoyu Tan: Research, data organization. Yuanhan Li: Research, data organization. Shiyao Xu: Research, data organization. Yujing Li: Manuscript review and editing, resource coordination. Qing Lin: Visualization, supervision, methodology. Fangyan He: Manuscript review and editing, resource coordination, methodology, conceptualization.

References

1. Ajoolabady A, Pratico D, Lin L et al (2024) Inflammation in atherosclerosis: Pathophysiology and mechanisms. Cell Death Dis 15:817. https://doi.org/10.1038/s41419-024-07166-8
2. Alugoju P, Vishnu Bhandare V, Patil S V, et al (2024) In silico molecular docking and molecular dynamic simulation of agarwood compounds with molecular targets of alzheimer's disease. https://doi.org/10.12688/f1000research.130618.2. F1000Research 12:230
3. Bahardoust M, Yarahmadi D, Aghakhani Z et al (2025) Comparison of short-term treatment with atorvastatin versus rosuvastatin for preventing contrast-associated acute kidney injury in patients undergoing coronary angiography/percutaneous coronary intervention: A systematic review and meta-analysis. J Cardiovasc Pharmacol. https://doi.org/10.1097/FJC.0000000000001718
4. Cai X, Tintut Y, Demer LL (2023) A potential new link between inflammation and vascular calcification. J Am Heart Assoc 12:e028358. https://doi.org/10.1161/JAHA.122.028358
5. Chen L, Chen S, Bai X et al (2024a) Low-density lipoprotein cholesterol, cardiovascular disease risk, and mortality in China. JAMA Netw Open 7:e2422558. https://doi.org/10.1001/jamanetworkopen.2024.22558
6. Chen X, Liu Y, Zhou Q et al (2024b) MiR-99a-5p up-regulates LDLR and functionally enhances LDL-C uptake via suppressing PCSK9 expression in human hepatocytes. Front Genet 15:1469094. https://doi.org/10.3389/fgene.2024.1469094
7. Clifford BL, Jarrett KE, Cheng J et al (2023) RNF130 regulates LDLR availability and plasma LDL cholesterol levels. Circ Res 132:849–863. https://doi.org/10.1161/CIRCRESAHA.122.321938
8. Dave T, Ezhilan J, Vasnawala H, Somani V (2013) Plaque regression and plaque stabilisation in cardiovascular diseases. Indian J Endocrinol Metab 17:983–989. https://doi.org/10.4103/2230-8210.122604
9. Ding X, Zheng L, Yang B et al (2019) Luteolin attenuates atherosclerosis via modulating signal transducer and activator of transcription 3-mediated inflammatory response. Drug Des Devel Ther 13:3899–3911. https://doi.org/10.2147/DDDT.S207185

10. Dou F, Chen J, Cao H et al (2019) Anti-atherosclerotic effects of LXRα agonist through induced conversion of M1 macrophage to M2. Am J Transl Res 11:3825–3840
11. Galeotti M, Orioles M, Saccà E et al (2023) Understanding the pathogenesis of red mark syndrome in rainbow trout (oncorhynchus mykiss) through an integrated morphological and molecular approach. Animals 13:1103. https://doi.org/10.3390/ani13061103
12. Guerguer FZ, Rossafi B, Abchir O et al (2025) Potential azo-8-hydroxyquinoline derivatives as multi-target lead candidates for alzheimer's disease: An in-depth in silico study of monoamine oxidase and cholinesterase inhibitors. PLoS ONE 20:e0317261. https://doi.org/10.1371/journal.pone.0317261
13. Guo X, Li B, Wen C et al (2023) TREM2 promotes cholesterol uptake and foam cell formation in atherosclerosis. Cell Mol Life Sci CMLS 80:137. https://doi.org/10.1007/s00018-023-04786-9
14. Guo Y, Yang J, He Y et al (2022) Protocatechuic aldehyde prevents ischemic injury by attenuating brain microvascular endothelial cell pyroptosis via lncRNA xist. Phytomedicine 94:153849. https://doi.org/10.1016/j.phymed.2021.153849
15. Handelsman Y, Lepor NE (2018) PCSK9 inhibitors in lipid management of patients with diabetes mellitus and high cardiovascular risk: a review. J Am Heart Assoc Cardiovasc Cerebrovasc Dis 7:e008953. https://doi.org/10.1161/JAHA.118.008953
16. Hosseini Faradonbeh SM, Seyedalipour B, Keivan Behjou N et al (2025) Structural insights into SOD1: From in silico and molecular dynamics to experimental analyses of ALS-associated E49K and R115G mutants. Front Mol Biosci 12:1532375. https://doi.org/10.3389/fmolb.2025.1532375
17. Hummelgaard S, Vilstrup JP, Gustafsen C et al (2023) Targeting PCSK9 to tackle cardiovascular disease. Pharmacol Ther 249:108480. https://doi.org/10.1016/j.pharmthera.2023.108480
18. Jeong GH, Kim KC, Lee JH (2025) Anti-inflammatory effects of cannabigerol in vitro and in vivo are mediated through the JAK/STAT/NFκB signaling pathway. Cells 14:83. https://doi.org/10.3390/cells14020083
19. Jia L, Qu P, Zhao Y et al (2025) Tripeptide DT-109 (gly-gly-leu) attenuates atherosclerosis and vascular calcification in nonhuman primates. Signal Transduct Target Ther 10:122. https://doi.org/10.1038/s41392-025-02201-2
20. Jimmy JL, Karn R, Kumari S et al (2023) Rice WRKY13 TF protein binds to motifs in the promoter region to regulate downstream disease resistance-related genes. Funct Integr Genomics 23:249. https://doi.org/10.1007/s10142-023-01167-0
21. Kong N, Xu Q, Cui W et al (2022) PCSK9 inhibitor inclisiran for treating atherosclerosis via regulation of endothelial cell pyroptosis. Ann Transl Med 10:1205. https://doi.org/10.21037/atm-22-4652
22. Li X, Li Z-F, Wu N-Q (2025a) Remnant cholesterol and residual risk of atherosclerotic cardiovascular disease. Rev Cardiovasc Med 26:25985. https://doi.org/10.31083/RCM25985
23. Li Y, Li X, Chen T et al (2025b) A programmable platelet theranostic platform for adaptive multi-stage delivery and synergistic immunotherapy in atherosclerosis. Nat Commun 16:6445. https://doi.org/10.1038/s41467-025-61789-9

24. Lightbody RJ, Taylor JMW, Dempsie Y, Graham A (2020) MicroRNA sequences modulating inflammation and lipid accumulation in macrophage foam cells: Implications for atherosclerosis. World J Cardiol 12:303–333. https://doi.org/10.4330/wjc.v12.i7.303
25. Magnussen C, Ojeda FM, Leong DP et al (2023) Global impact of modifiable risk factors on cardiovascular disease and mortality. N Engl J Med 389:1273–1285. https://doi.org/10.1056/NEJMoa2206916
26. Park T, Workun B Further evidence to support weight loss and lifestyle interventions for people taking antipsychotic medications. Evid Based Ment Health 18:128. https://doi.org/10.1136/eb-2015-102068
27. Pickett JR, Wu Y, Zacchi LF, Ta HT (2023) Targeting endothelial vascular cell adhesion molecule-1 in atherosclerosis: Drug discovery and development of vascular cell adhesion molecule-1–directed novel therapeutics. Cardiovasc Res 119:2278–2293. https://doi.org/10.1093/cvr/cvad130
28. Shi X, Gao J, Lv Q et al (2020) Calcification in atherosclerotic plaque vulnerability: Friend or foe? Front Physiol 11:56. https://doi.org/10.3389/fphys.2020.00056
29. Shi Y, Dong L, Ju Z et al (2023) Exploring potential SARS-CoV-2 mpro non-covalent inhibitors through docking, pharmacophore profile matching, molecular dynamic simulation, and MM-GBSA. J Mol Model 29:138. https://doi.org/10.1007/s00894-023-05534-3
30. Soehnlein O, Libby P (2021) Targeting inflammation in atherosclerosis — from experimental insights to the clinic. Nat Rev Drug Discov 20:589–610. https://doi.org/10.1038/s41573-021-00198-1
31. Toth PP, Banach M (2024) It is time to address the contribution of cholesterol in all apoB-containing lipoproteins to atherosclerotic cardiovascular disease. Eur Heart J Open 4:oeae057. https://doi.org/10.1093/ehjopen/oeae057
32. Vinolo-Gil MJ, Herrera-Sánchez C, Martin-Vega FJ et al Eficacia de la tele-rehabilitación en pacientes con enfermedad pulmonar obstructiva crónica: Una revisión sistemática. Sist Sanit Navar 45:e0999. https://doi.org/10.23938/ASSN.0999
33. Wang K, Bai X, Mei L et al (2022) CircRNA_0050486 promotes cell apoptosis and inflammation by targeting miR-1270 in atherosclerosis. Ann Transl Med 10:905. https://doi.org/10.21037/atm-22-3745
34. Wei X, Zhang Y, Xie L et al (2021) Pharmacological inhibition of EZH2 by GSK126 decreases atherosclerosis by modulating foam cell formation and monocyte adhesion in apolipoprotein E-deficient mice. Exp Ther Med 22:841. https://doi.org/10.3892/etm.2021.10273
35. Xu K, Saaoud F, Yu S et al (2022) Monocyte adhesion assays for detecting endothelial cell activation in vascular inflammation and atherosclerosis. Methods Mol Biol Clifton NJ 2419:169–182. https://doi.org/10.1007/978-1-0716-1924-7_10
36. Yang R, Zhang L, Bu F et al (2024) AI-based prediction of protein–ligand binding affinity and discovery of potential natural product inhibitors against ERK2. BMC Chem 18:108. https://doi.org/10.1186/s13065-024-01219-x

37. Zhang L, Li Y, Yang W et al (2023) Protocatechuic aldehyde increases pericyte coverage and mitigates pericyte damage to enhance the atherosclerotic plaque stability. Biomed Pharmacother 168:115742. https://doi.org/10.1016/j.biopha.2023.115742
38. Atherosclerosis and inflammation: are the rules of the game changing with biological therapies? - PMC. https://pmc.ncbi.nlm.nih.gov/articles/PMC12302978/. Accessed 7 Nov 2025a
39. Fibroblast growth factor-2/platelet-derived growth factor enhances atherosclerotic plaque stability - mao – 2020 - journal of cellular and molecular medicine - wiley online library. https://onlinelibrary.wiley.com/doi/10.1111/jcmm.14850. Accessed 17 Oct 2025b

Figures

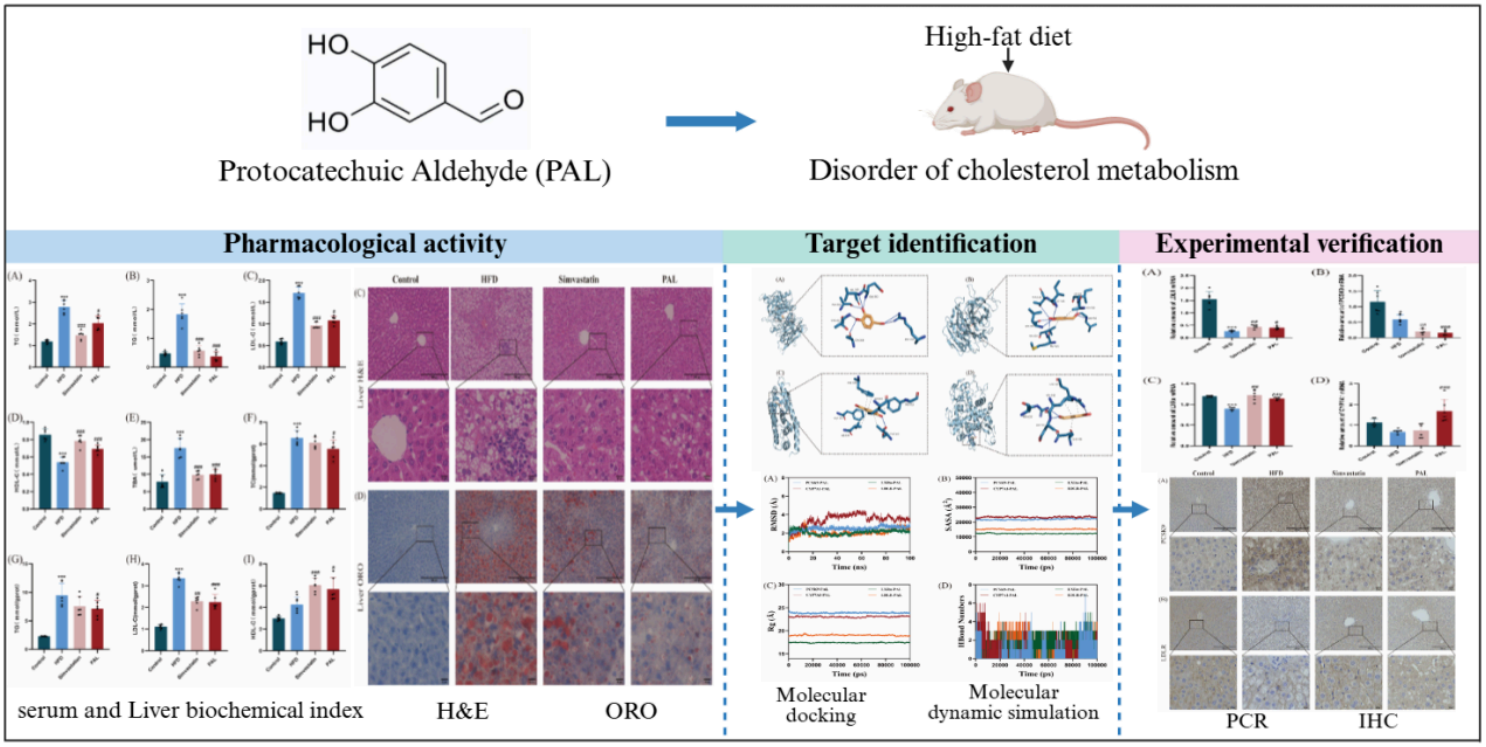


Figure 1

Graphical abstract

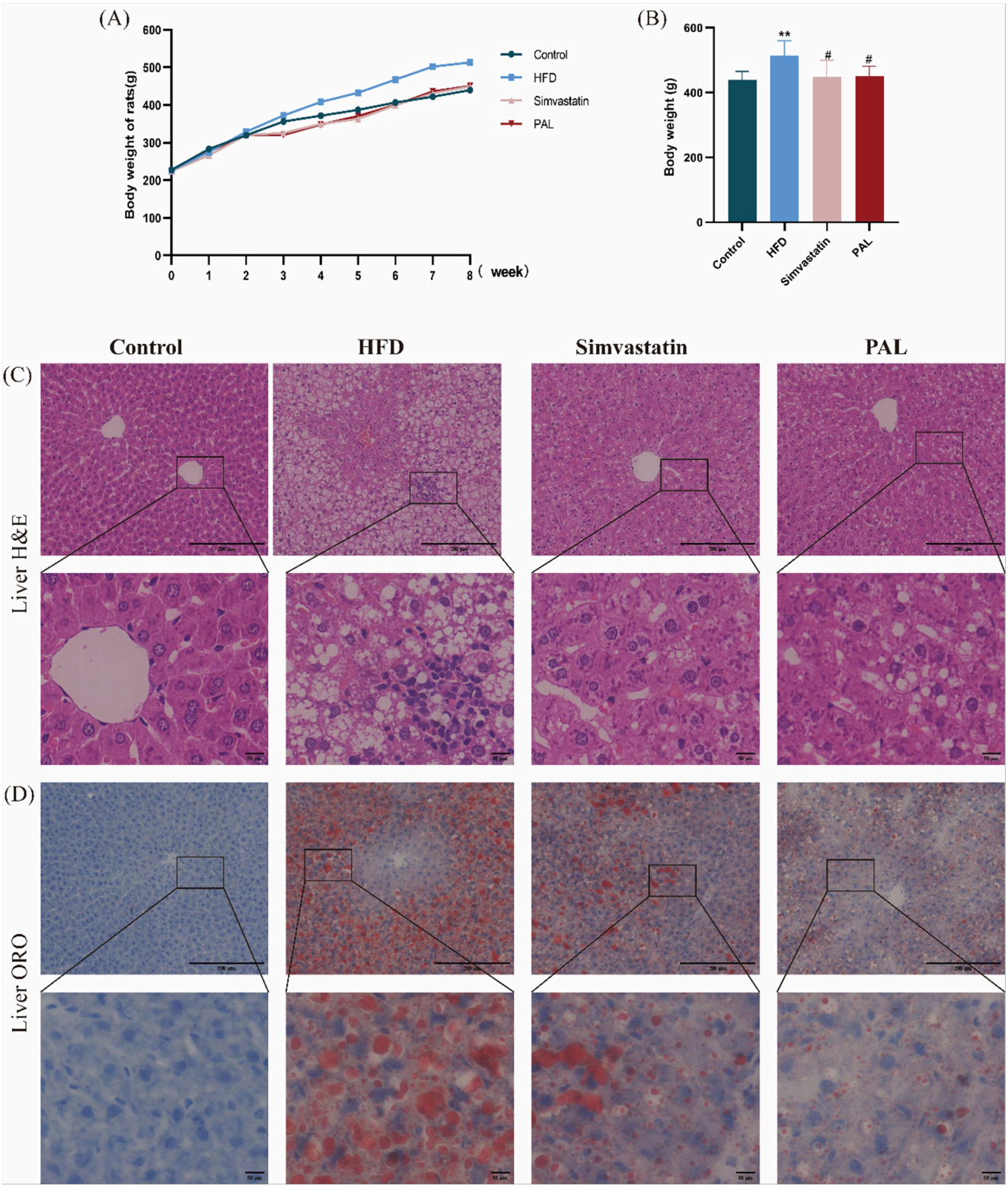


Figure 2

PAL alleviates hepatic steatosis in HFD rats. (A) Body weight changes in rats from each group during the experiment. (B) Body weight changes at the end of treatment. Representative images of liver tissue. (C) H&E staining. (D) Oil red O staining (Scale bar: 200 μm and 50 μm). Data are expressed as mean ± SD (n = 6). $^{**}P < 0.01$ compared with control group, $^{\#}P < 0.05$ compared with HFD group.

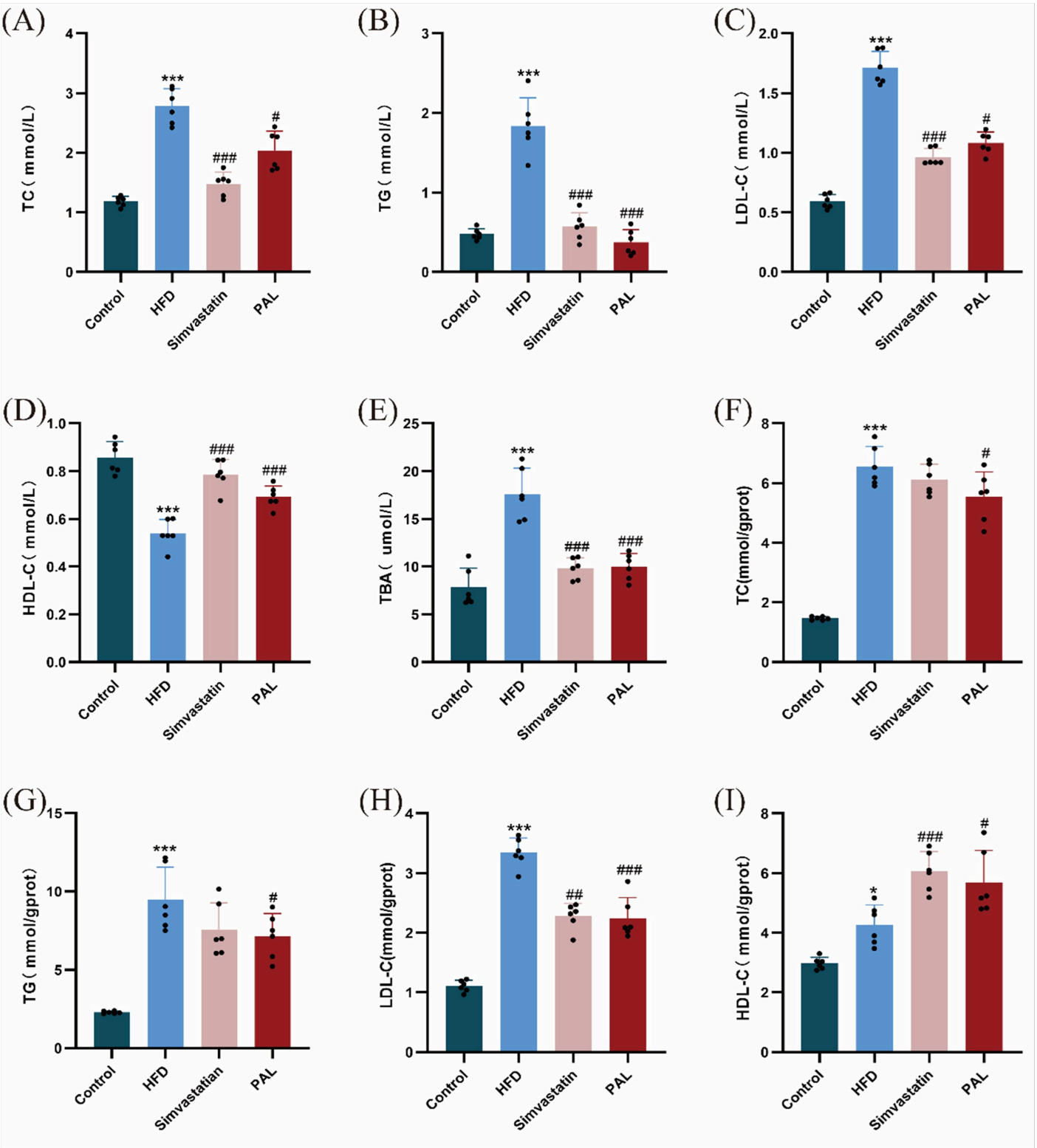


Figure 3

PAL modulates cholesterol metabolism in HFD-fed rats. Serum levels of TC (A), TG (B), LDL-C (C), HDL-C (D), and TBA (E). Hepatic levels of TC (F), TG (G), LDL-C (H), and HDL-C (I). Data are presented as mean ± SD (n = 6). $^{*}P < 0.05$, $^{***}P < 0.001$ vs. control group; $^{\#}P < 0.05$, $^{\#\#}P < 0.01$, $^{\#\#\#}P < 0.001$ vs. HFD group.

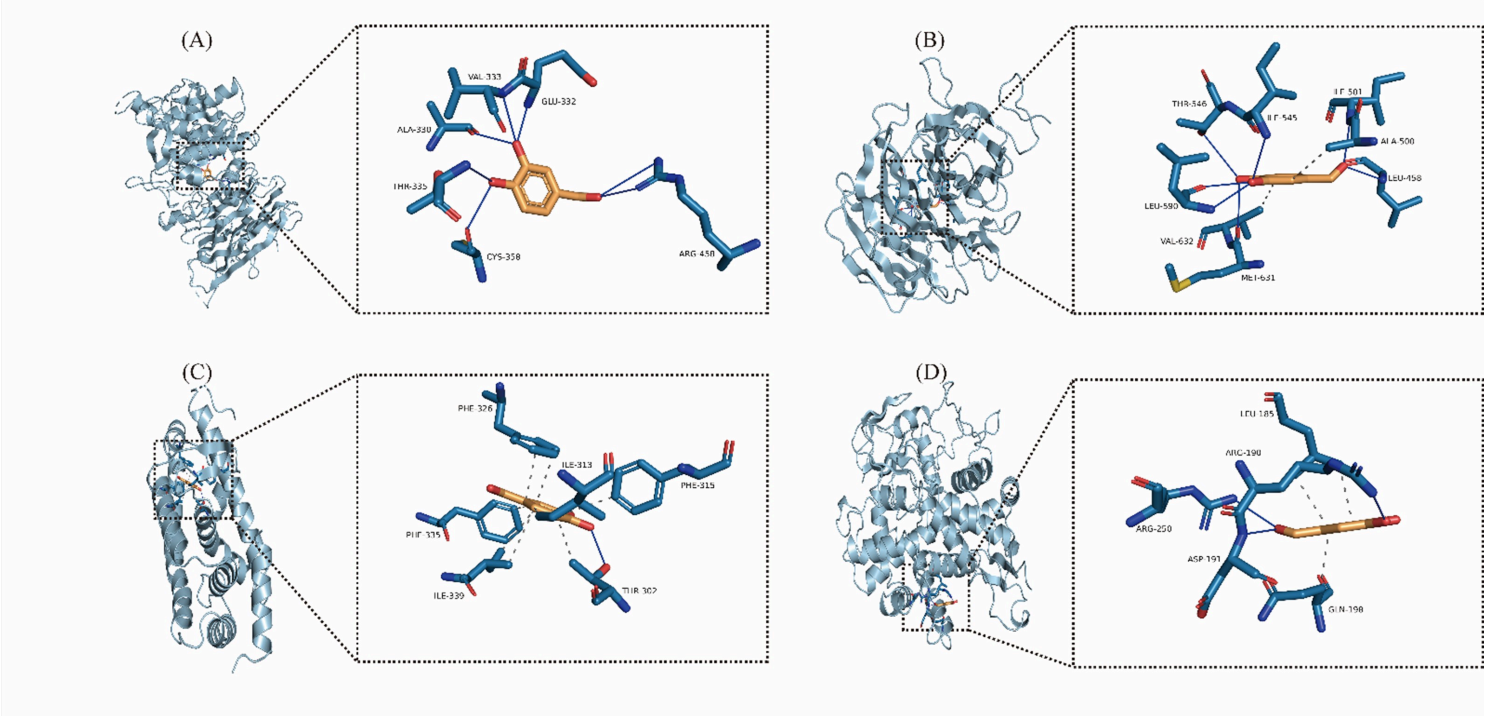


Figure 4

Molecular interactions between (A) PAL and PCSK9, (B) PAL and LDLR, (C) PAL and LXRα, and (D) PAL and CYP7A1.

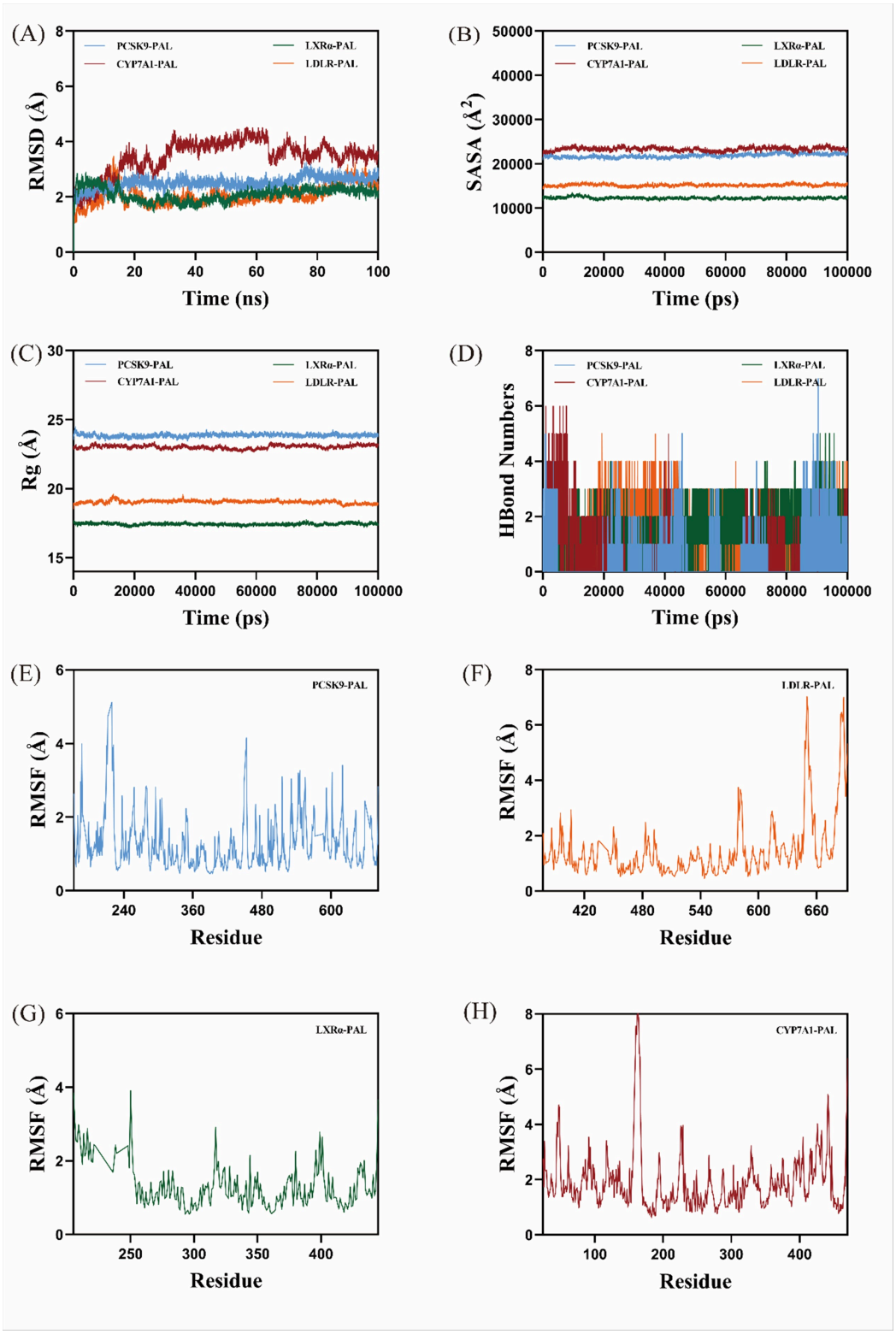


Figure 5

Molecular dynamics simulation results. (A) RMSD trajectories of PCSK9, LDLR, LXRα, CYP7A1, and PAL over the 100 ns simulation period. (B) SASA profiles of PCSK9, LDLR, LXRα, CYP7A1, and PAL over time. (C) Rg values for PCSK9, LDLR, LXRα, CYP7A1, and PAL over time. (D) Hydrogen bonds between PCSK9, LDLR, LXRα, CYP7A1, and PAL over time. (E–H) RMSF values of amino acid backbone atoms in PCSK9 (E), LDLR (F), LXRα (G), and CYP7A1 (H) in complex with PAL.

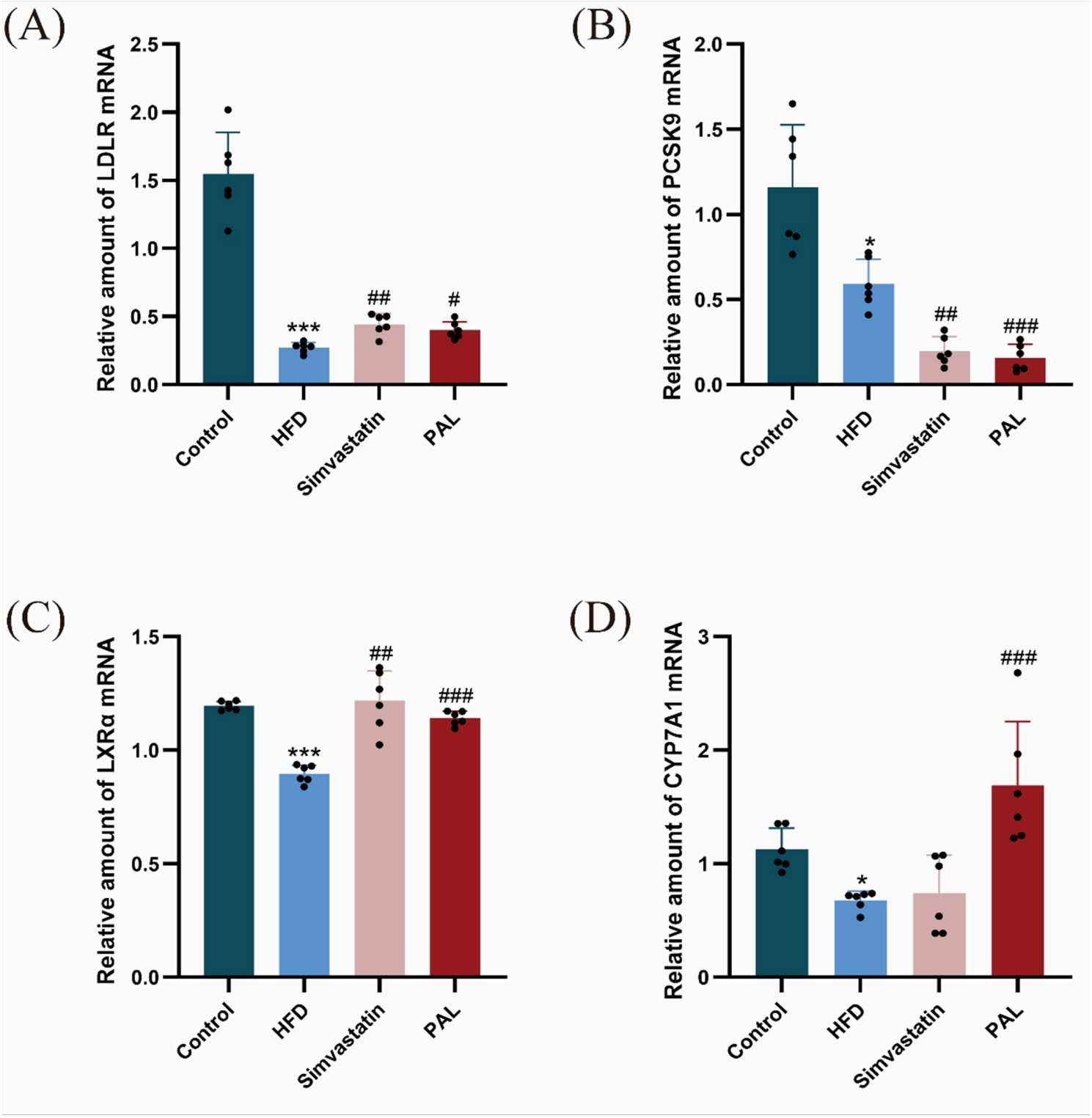


Figure 6

PAL modulates cholesterol metabolism by influencing hepatic mRNA levels of LDLR, LXRα, CYP7A1, and PCSK9. Relative mRNA expression levels of PCSK9 (A), LDLR (B), LXRα (C), and CYP7A1 (D) in the liver. Data are presented as mean ± SD. $^{*}P < 0.05$, $^{***}P < 0.001$ vs. control group; $^{\#}P < 0.05$, $^{\#\#}P < 0.01$, $^{\#\#\#}P < 0.001$ vs. HFD group.

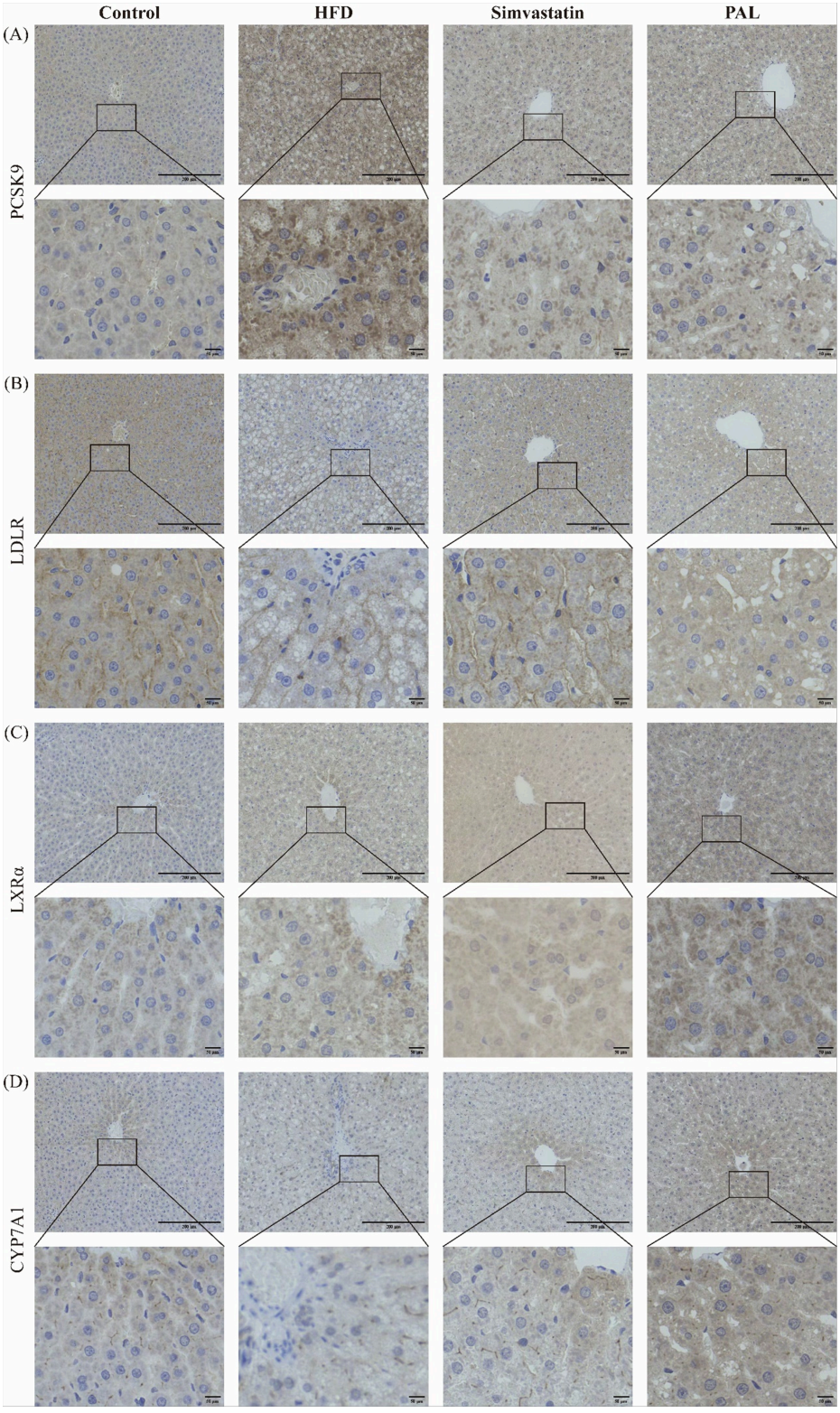


Figure 7

PAL modulates cholesterol metabolism by influencing hepatic protein levels of LDLR, LXRα, CYP7A1, and PCSK9. Protein expression levels of PCSK9 (A), LDLR (B), LXRα (C), and CYP7A1 (D) in the liver.